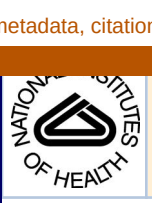

Published in final edited form as:

Dalton Trans. 2014 December 2; 44(1): 119–129. doi:10.1039/c4dt02627f.

Oxidative Halogenation of Cisplatin and Carboplatin: Synthesis, Spectroscopy, and Crystal and Molecular Structures of Pt(IV) Prodrugs

Timothy C. Johnstone[a], **Sarah M. Alexander**[a], **Justin J. Wilson**[a], and **Stephen J. Lippard**[*]

[a] Department of Chemistry, Massachusetts Institute of Technology, Cambridge, Massachusetts 02139, United States

Abstract

A series of Pt(IV) prodrugs has been obtained by oxidative halogenation of either cisplatin or carboplatin. Iodobenzene dichloride is a general reagent that cleanly provides prodrugs bearing axial chlorides without the need to prepare intervening Pt(IV) intermediates or handle chlorine gas. Elemental bromine and iodine afford Pt(IV) compounds as well, although in the case of the iodine-mediated oxidation of carboplatin, an amido-bridged Pt(IV) side product also formed. A detailed analysis of the changes in spectroscopic and structural parameters induced by varying the axial halide is presented. A number of recurring motifs are observed in the solid state structures of these compounds.

Introduction

Platinum complexes play a significant role in the clinical treatment of cancer, with cisplatin, carboplatin, and oxaliplatin (Chart 1) comprising one of the most widely prescribed classes of antineoplastic drugs.[1] These three coordination complexes feature platinum in the 2+ oxidation state. Indeed, this oxidation state, and the square-planar coordination geometry that platinum(II) almost invariably adopts, long dominated the landscape of platinum drug development. Despite the monopoly that Pt(II) holds over the market for platinum-based drugs, platinum(IV) complexes also have biological activity, as revealed in some of the earliest experiments.[2] Pt(IV) compounds were extensively pursued in preclinical and clinical settings early in the history of this class of drugs (Chart 1).[3] The status of satraplatin (Chart 1) was closely monitored as it progressed through clinical trials, although it ultimately failed to achieve the desired increased lifespan when used in combination with prednisone for treatment of hormone-refractory prostate cancer.[4]

Pt(IV) compounds as a class act as prodrugs that undergo intracellular reduction to yield active Pt(II) species, which can proceed to bind nuclear DNA and initiate a cellular response that eventually triggers cell death pathways.[5] Pt(IV) prodrugs typically contain the four

lippard@mit.edu.

Electronic Supplementary Information (ESI) available: NMR spectra, crystallographic parameters, and Cartesian coordinates of calculated structures. See DOI: 10.1039/b000000x/

ligands of a Pt(II) precursor of known anticancer activity arranged in a square-planar geometry with two additional ligands, disposed trans to one another, completing the octahedral coordination sphere.[6] Although it is widely stated that reduction of Pt(IV) prodrugs proceeds with loss of these two additional, so-called “axial” ligands, recent studies reveal that other reduction products are possible.[7,8] The nature of the ligands bound to the Pt(IV) center significantly influences the mechanism and kinetics of reduction.[9,10]

Most Pt(IV) prodrugs bear axial chloride, hydroxide, or carboxylate ligands because of the synthetic ease with which they can be installed.[11] Oxidation of a Pt(II) complex with hydrogen peroxide in water typically affords the Pt(IV) derivative with two trans hydroxide ligands in which the relative geometry of the ligands bound originally to the metal center remains undisturbed. The metal-bound hydroxide ligands are sufficiently nucleophilic to attack carboxylic acid anhydrides to yield Pt(IV) carboxylates.[11] Similar nucleophilic attack of other substrates can afford Pt(IV) carbonates and carbamates.[12,13] Treatment with hydrochloric acid results in substitution of the hydroxide ligands for chloride, presumably through an intermediate bearing aqua ligands.[14] Pt(IV) prodrugs with chloride axial ligands can also be obtained by direct oxidation with chlorine gas.[15]

In the course of exploring the chemistry of Pt(IV) prodrugs, the oxidative halogenation of cisplatin and carboplatin was investigated with the aim of expanding the range of commonly encountered axial ligands and the synthetic methodologies for accessing them (Chart 2). We found iodobenzene dichloride to be a suitable replacement for chlorine gas in the preparation of prodrugs with axial chloride ligands. Bromine and iodine are more suitable than chlorine for laboratory handling and provided ready access to prodrugs having axial bromide and iodide ligands, respectively. An unexpected dimerization occurred as a side reaction upon treatment of carboplatin with I_2. Here we report details of the synthesis and characterization of these compounds and anticipate that these reactions will be readily applicable to the preparation of Pt(IV) prodrugs from other biologically active Pt(II) complexes. The crystal structures of several of these prodrugs, as well as those of related platinum complexes, were determined, salient features of which are discussed.

Experimental

General considerations

Unless otherwise specified, reactions were conducted in a fume hood with protection from light. Reactions leading to the formation of the Pt(IV) iodide complexes were particularly prone to photodecomposition. All reagents were used as received from commercial vendors without further purification. Carboplatin was prepared as previously described.[16] *cis,trans*-[Pt(CBDCA)$(NH_3)_2(OH)_2$], where CBDCA is 1,1-cyclobutane-dicarboxylate, was prepared as previously reported.[17]

Physical Measurements

^1H, ^{13}C, ^{14}N, or ^{195}Pt NMR spectra were acquired on either a Varian Inova-500 or a Bruker DPX-400 spectrometer in the MIT Department of Chemistry Instrumentation Facility (DCIF) at room temperature. Resonant absorptions are reported as chemical shifts (δ) in ppm with respect to tetramethylsilane (^1H and ^{13}C), NH_4Cl (^{14}N), or Na_2PtCl_6 (^{195}Pt).

NMR spectra were referenced to residual solvent signals (^{1}H and ^{13}C), an external solution of NH_4Cl in 0.1 M HCl (^{14}N δ = 0 ppm), or an external solution of K_2PtCl_4 in D_2O (^{195}Pt δ = −1628 ppm). ^{14}N NMR spectra were acquired for 1 and 2 but not 3–6.[18] Elemental analyses for the previously unreported compounds 4–6 were provided by a commercial laboratory. Combustion analyses were not carried out for the known compounds 1–3.

Synthesis of iodobenzene dichloride

The synthesis is a modification of that previously reported.[19] Iodobenzene (250 mg, 1.22 mmol) was suspended in household bleach (10 mL, 5.25% NaClO). Concentrated hydrochloric acid was added in a dropwise manner until gas evolution ceased (ca. 2 mL). The resulting yellow precipitate was collected by filtration, washed with water (3 × 10 mL), air dried, and washed with hexanes (3 × 10 mL). The solid was dissolved in a minimal amount of hot chloroform and cooled to room temperature. The solution was allowed to stand at −40 °C overnight. Yellow needles formed and were collected by filtration, washed with hexanes, and dried in vacuo for 2 h. Yield 240 mg, 72%. Spectroscopic characterization matches that previously reported.[19]

Synthesis of *cis*-[Pt(NH$_3$)$_2$Cl$_4$] (1)

Cisplatin (100 mg, 0.33 mmol) was suspended in DMF (2 mL). A solution of iodobenzene dichloride (92 mg, 0.33 mmol) in DMF (1 mL) was added to the cisplatin suspension. The color of the suspension briefly turned deep orange, but quickly lightened to a bright yellow and all of the solids dissolved. The mixture was stirred at room temperature for 10 min followed by addition of diethyl ether (30 mL) to precipitate a yellow solid. The solid was collected by filtration, washed with diethyl ether, and dried in vacuo. Yield: 121 mg, 99%. M.p. 220–230 °C (dec). ^{1}H NMR (500 MHz, DMF-d_7) δ 5.87 ($^{1}J_{H–N}$ = 55 Hz, $^{2}J_{H–Pt}$ = 50 Hz). ^{1}H NMR (400 MHz, DMSO-d_6) δ 5.83 ($^{1}J_{H–N}$ = 52 Hz, $^{2}J_{H–Pt}$ = 56 Hz). ^{14}N NMR (28.9 MHz, DMSO-d_6) δ –33.7 ($^{1}J_{N–H}$ = 53 Hz, $^{1}J_{N–Pt}$ = 177 Hz). ^{195}Pt NMR (108 MHz, DMF-d_7) δ –257. ^{195}Pt NMR (86 MHz, DMSO-d_6) δ –127.

Synthesis of *cis,cis,trans*-[Pt(NH$_3$)$_2$Cl$_2$Br$_2$] (2)

Cisplatin (100 mg, 0.33 mmol) was suspended in DMF (2 mL). A solution of bromine (53 mg, 0.33 mmol) in DMF (1 mL) was added to the cisplatin suspension. The mixture was stirred at room temperature for 10 min. Addition of diethyl ether (15 mL) resulted in precipitation of an orange solid. The solid was collected by filtration, washed with diethyl ether, and dried in vacuo. Yield: 121 mg, 80%. M.p. 200–220 °C (dec). ^{1}H NMR (400 MHz, DMSO-d_6) δ 5.77 ($^{1}J_{H–N}$ = 52 Hz, $^{2}J_{H–Pt}$ = 52 Hz). ^{14}N{^{1}H} NMR (28.9 MHz, DMSO-d_6) δ −40.9 ($^{1}J_{N–Pt}$ = 175 Hz). ^{195}Pt NMR (86 MHz, DMSO-d_6) δ −732 ($^{1}J_{Pt–N}$ = 175 Hz, $^{2}J_{Pt–H}$ = 50 Hz).

Synthesis of *cis,cis,trans*-[Pt(NH$_3$)$_2$Cl$_2$I$_2$] (3)

Cisplatin (100 mg, 0.33 mmol) was suspended in DMF (2 mL). A solution of iodine (84 mg, 0.33 mmol) in DMF (2 mL) was added to the cisplatin suspension. The mixture was stirred at room temperature for 10 min. Addition of diethyl ether (25 mL) resulted in precipitation of a red-purple solid. The solid was collected by filtration, washed with diethyl ether, and

dried in vacuo. Yield: 133 mg, 73%. M.p. 205–218 °C (dec). ^{1}H NMR (500 MHz, DMF-d_7) δ 5.77 ($^{1}J_{H–N}$ = 53 Hz). ^{195}Pt NMR (108 MHz, DMF-d_7) δ −1866.

Synthesis of *cis,trans*-[Pt(CBDCA)(NH$_3$)$_2$Cl$_2$] (4)

Carboplatin (100 mg, 0.27 mmol) was suspended in DMF (6 mL). A solution of iodobenzene dichloride (83 mg, 0.30 mmol) in DMF (2 mL) was added to the carboplatin suspension. The mixture was stirred at 75 °C for 30 min after which time the solid was consumed producing a yellow solution. The solution was concentrated under vacuum to a volume of approximately 5 mL. Methanol (1 mL) was added and the solution was filtered through Celite. Addition of diethyl ether (15 mL) resulted in precipitation of a yellow solid. The solid was collected by filtration, washed with diethyl ether, and dried in vacuo. Yield: 97 mg, 85%. M.p. 167–173 (dec). ^{1}H NMR (500 MHz, DMF-d_7) δ 6.10 (6H, m, $^{1}J_{H–N}$ = 50 Hz, $^{2}J_{H–Pt}$ = 45 Hz), 2.59 (4H, t, $^{3}J_{H–H}$ = 8 Hz), 1.88 (2H, p, $^{3}J_{H–H}$ = 8 Hz). ^{13}C NMR (125 MHz, DMSO-d_6) δ 176.5, 55.8, 31.8, 15.6. ^{195}Pt NMR (108 MHz, DMF-d_7) δ 761. Anal. calcd for $C_{12}H_{26}Cl_2N_4O_6Pt$: C 24.50, H 4.45, N 9.52; found: C 24.07, H 4.13, N 9.66.

Synthesis of *cis,trans*-[Pt(CBDCA)(NH$_3$)$_2$Br$_2$] (5)

Carboplatin (150 mg, 0.40 mmol) was suspended in DMF (2 mL) and a solution of bromine (65 mg, 0.40 mmol) in DMF (1 mL) was added. The mixture was stirred at room temperature for 30 min and then at 50 °C for an additional 10 min, after which time the solid was consumed producing an orange solution. The mixture was filtered through Celite and addition of the filtrate to diethyl ether (150 mL) resulted in precipitation of an orange solid. The solid was collected by filtration, washed with diethyl ether, and dried in vacuo. Yield: 181 mg, 84%. M.p. 169–172 °C (dec). ^{1}H NMR (500 MHz, DMF-d_7) δ 6.01 (6H, m, $^{1}J_{H–N}$ = 52 Hz, $^{2}J_{H–Pt}$ = 45 Hz), 2.60 (4H, t, $^{3}J_{H–H}$ = 10 Hz), 1.89 (2H, p, $^{3}J_{H–H}$ = 10 Hz). ^{13}C NMR (125 MHz, DMSO-d_6) δ 176.6, 56.0, 31.8, 15.5. ^{195}Pt NMR (108 MHz, DMF-d_7) δ 229 ($^{1}J_{Pt–N}$ = 150 Hz). Anal. calcd for $C_6H_{12}Br_2N_2O_4Pt$·0.3DMF (supported by NMR integration): C 14.99, H 2.57, N 5.83; found: C 15.32, H 2.49, N 5.33.

Oxidation of carboplatin with I$_2$

Carboplatin (100 mg, 0.27 mmol) was suspended in DMF (2 mL). A solution of iodine (70 mg, 0.27 mmol) in DMF (3 mL) was added to the carboplatin suspension. The mixture was stirred at room temperature for 30 min, during which time a yellow solid began to form. Addition of diethyl ether (5 mL) induced precipitation of more yellow solid and the mixture was cooled at 4 °C for 1 h. The yellow solid was collected by filtration and washed with cold DMF (8 mL) and diethyl ether (15 mL). Spectroscopic and crystallographic analysis revealed this substance to be the amido-bridged dimer [Pt(CBDCA)I(NH$_3$)(μ-NH$_2$)]$_2$ (7). The red-purple filtrate was added to 100 mL of rapidly stirring diethyl ether to precipitate a red-brown solid. The solid was collected by filtration, washed with diethyl ether, and dried under vacuum. The spectroscopic properties of this complex are consistent with its formulation as 6. Yield: 108 mg, 64%. M.p. 164–180 °C (dec). ^{1}H NMR (500 MHz, DMF-d_7) δ 6.25 (6H, m, $^{1}J_{H–N}$ = 52 Hz, $^{2}J_{H–Pt}$ = 50 Hz), 2.67 (4H, t, $^{3}J_{H–H}$ = 7.5 Hz), 1.90 (2H, p, $^{3}J_{H–H}$ = 7.5 Hz). ^{13}C NMR (125 MHz, DMF-d_7) δ 178.3, 58.1, 33.1, 16.6. ^{195}Pt NMR

(108 MHz, DMF-d_7) δ –856. Anal. calcd for $C_{12}H_{26}I_2N_4O_6Pt$: C 18.69, H 3.40, N 7.26; found: C 18.75, H 3.18, N 7.20.

X-ray crystallography

Crystals of 1, 3, 4, and 5 were obtained by allowing diethyl ether vapor to diffuse into a DMF solution of the compound. The DMF-diethyl ether solvate of 1 was obtained in a similar manner, whereas the DMSO solvate of 1 was obtained by layering toluene onto a DMSO solution of the compound. Crystallization vials containing spectroscopically pure 1 and 3 were left to stand at room temperature for more than two months and afforded crystals of the decomposition products *fac*-$[Pt(NH_3)_3Cl_3]Cl$ and *fac*-$[Pt(NH_3)_3Br_3]Br$. Crystals of 7 were obtained directly from the reaction mixture and those of *cis,trans*-$[Pt(CBDCA)(NH_3)_2(OH)_2]$ were formed by recrystallization from hot water. Samples suitable for X-ray diffraction were selected microscopically under crossed polarizers, mounted on a nylon loop in Paratone oil, and cooled to 100 K under a stream of nitrogen. Diffraction was carried out on a Bruker APEX CCD X-ray diffractometer controlled by the *APEX2* software using Mo Kα radiation (λ = 0.71073 Å).[20] The data were integrated with *SAINT*[21] and absorption, Lorentz, and polarization corrections were calculated by *SADABS*.[22] Space group determination was carried out by analyzing the Laue symmetry and the systematically absent reflections with *XPREP*.[23] Structures were solved by direct or heavy atom methods and refinement was performed with the *SHELX-97* program suite.[24] Refinement was carried out against F^2 using standard procedures.[25] Non-hydrogen atoms were located in difference Fourier maps and refined anisotropically. Hydrogen atoms were placed at calculated positions and refined using a riding model unless otherwise specified in the corresponding CIF (see Electronic Supporting Information, ESI). For coordinated NH_3 and terminal CH_3 groups, hydrogen atom isotropic displacement parameters (U_{iso}) were set equal to 1.5 times the U_{iso} of the atom to which they were attached. For other hydrogen atoms, U_{iso} = 1.2 U_{iso} of the attached atom. The details of any restraints employed are presented in the corresponding CIF (see ESI). All structures were checked for missed higher symmetry and twinning with *PLATON* and were further validated using *CheckCIF*.[26] Least-squares planes were fit using *XP* and visualized using *Mercury*.[24,27] Refinement details are presented in Table 1 and depictions of the molecular structures of the platinum complexes from their respective crystal structures are shown in Fig. 1.

Computational details

DFT calculations were executed with *Gaussian 03*.[28] The PBE0 hybrid functional was employed.[29] The valence electrons of the Pt, Br, and I atoms were treated using the LANL2DZ basis set and relativistic effects were taken into consideration by employing the corresponding LANL2DZ effective core potentials.[30,31] The Pople-type 6-31++g(d,p) basis set was used for all other atoms.[32,33] Geometry optimizations were carried out for 4, 5, and 6 in the gas phase followed by analytical frequency calculations. The lack of imaginary frequencies in the latter was used as confirmation that the converged-upon geometry is indeed a minimum on the potential energy surface of the molecule. Comparison of the optimized gas-phase structures to the crystallographically determined molecular structures was performed using *Mercury*.[27] Cartesian coordinates for all optimized structures are provided in the ESI.

Results and discussion

Oxidative halogenation of cisplatin

The oxidation of an aqueous suspension of cisplatin with chlorine to form 1 has been previously reported,[15] as has oxidation of cisplatin with bromine water to afford 2,[34] but to the best of our knowledge the oxidation of cisplatin using iodine to yield 3 has not been described. We report here a general procedure to obtain Pt(IV) trans dihalide complexes by treating DMF solutions of the parent platinum(II) compounds with stoichiometric amounts of oxidant, followed by precipitation with diethyl ether.

The methods most widely employed in the literature to prepare Pt(IV) prodrugs bearing axial chlorides involve oxidation of the Pt(II) precursor with Cl_2 or with hydrogen peroxide in water to afford the dihydroxide complex followed by treatment with hydrochloric acid.[11] An alternative reaction that in one step both oxidizes and chlorinates the platinum center is treatment with PCl_5. Phosphorus pentachloride was used to convert [Pt(en)I_2] to *cis,trans*-[Pt(en)I_2Cl_2].[35] The use of the mono-chlorinating oxidant N-chlorosuccinimide in the preparation of prodrugs bearing one axial chloride has very recently been described.[36] In only a few reports have we and others used iodobenzene dichloride in the preparation of platinum anticancer agents bearing axial trans chlorides.[11,37-40]

Iodobenzene dichloride is readily prepared in a robust reaction using iodobenzene, household bleach, and hydrochloric acid.[19] Contrary to previous reports of the long term instability of this reagent,[41-43] we find it to be stable for up to one year if recrystallized from chloroform and stored at −40 °C. It can be handled readily in air at room temperature during the course of setting up reactions. Moreover, the by-product, iodobenzene, is highly soluble in a solvent such as diethyl ether, which is used here to precipitate the desired platinum-containing products.

When a DMF solution of cisplatin is treated with a DMF solution of iodobenzene dichloride, a rapid color change occurs. If the solutions are dilute, the change is marked by a brightening of the yellow coloration. If the DMF solutions are at concentrations approaching saturation, the reaction mixture initially turns an intense orange, which rapidly converts to bright yellow. We have not investigated the details of this reaction, but it is possible that at high concentrations a dimeric Pt(III) intermediate may form that is subsequently cleaved.[11] Alternatively, a Pt(IV) intermediate may form in which a solvent molecule is bound trans to the initially added chloride. This solvent ligand would then be displaced by the chloride ion that is liberated on reduction of the I(III) center in iodobenzene dichloride to I(I). Similar solvent-ligated intermediates in the Cl_2 oxidation of platinum(II) complexes were spectroscopically observed and crystallographically characterized.[44-46]

Unlike chlorine, bromine and iodine are more readily handled at ambient temperature and pressure and so alternative reagents to carry out oxidative bromination and iodination were not sought. Oxidation of cisplatin with bromine to form **2** proceeded smoothly as did oxidation with iodine to yield **3**. Deeply colored, **3** was particularly sensitive to photodecomposition when the oxidation was performed without exclusion of light. The nature of the decomposition products was not investigated in detail but we note that others

have exploited the photoreactivity of Pt(IV) iodide complexes to design photoactivated Pt(IV) prodrugs.[35,47] A detailed description of the spectroscopic and crystallographic properties of **1**–**3** is presented below.

Oxidative halogenation of carboplatin

The oxidation of carboplatin with iodobenzene dichloride and elemental bromine produced 4 and 5 in a manner analogous to the corresponding oxidations of cisplatin. We note that, in contrast to the iodobenzene dichloride oxidation of cisplatin, no transient red coloration of the reaction was observed. If the colored intermediate is a Pt–Pt bonded species, then the bulky CBDCA ligand may preclude its formation. A detailed description of the spectroscopic and crystallographic properties of 4 and 5 is presented below. Combination of a DMF solution of iodine and a suspension of carboplatin initially produced a homogenous solution. After a few minutes, a yellow solid appeared in the reaction mixture and addition of diethyl ether induced further precipitation of a small amount of yellow microcrystalline solid, which was removed by filtration. Further dilution of the filtrate with diethyl ether afforded 6 as a dark red-brown solid.

^{1}H NMR spectroscopic analysis of the yellow solid initially formed in the reaction showed, in addition to signals corresponding to unreacted carboplatin, the presence of two resonances centered at 6.03 and 4.75 ppm, another at 1.83 ppm, and a final one buried under the DMSO solvent peak (Fig. S22, ESI). The two most upfield signals exhibit splitting consistent with that expected for the resonances of a CBDCA ligand. The remaining two resonances occur downfield of where the ammine signals from carboplatin appear, consistent with terminal ammines or bridging amides bound to a Pt(IV) center.[48,49] The integrated intensities of these downfield resonances indicate that they arise from three and two protons, respectively, when compared to the integrated intensities of those arising from the cyclobutane fragment of the CBDCA ligand. Moreover, the yellow color of the product differed significantly from the red or purple hue that would be expected for the desired diiodide compound. X-ray crystallographic analysis revealed the species to be the amido-bridged dimer $[Pt(CBDCA)I(NH_3)(\mu\text{-}NH_2)]_2$, which is consistent with these ^{1}H NMR spectral data. A detailed description of the structure of this species is presented below.

NMR spectroscopic trends

Spectroscopic investigation of the compounds reported here not only provides a means of confirming their identities but also reveals trends as the halide ligands are varied. The ^{1}H NMR spectral signals of the NH_3 ligands of 1–6 show a characteristic splitting pattern induced by coupling to both ^{195}Pt (I = ½) and quadrupolar ^{14}N (I = 1). Whereas ^{14}N exhibits 99.6% natural abundance, ^{195}Pt is only 33.8% abundant. Two-bond coupling of the ammine protons to the ^{195}Pt nucleus produces additional satellite peaks. Resolution of these coupling effects is often complicated by broadening from quadrupolar relaxation of ^{14}N and chemical shift anisotropy (CSA) of ^{195}Pt. The former is greatly reduced upon oxidation of Pt(II) to Pt(IV) because of symmetrization of the electric field gradient at the ^{14}N nucleus.[39] The CSA of the platinum nucleus is also greatly reduced on transitioning from square-planar Pt(II) to octahedral Pt(IV).[50] The combination of these two effects allows coupling to be readily observed. Coupling of ^{1}H to both ^{14}N and ^{195}Pt is expected to produce 1:1:1 triplet,

each component of which will bear satellite peaks. The coupling constants of the two interactions happen to be approximately equal, which positions the satellite peaks of the inner member of the 1:1:1 triplet directly over those of the outer members of the triplet. The pattern experimentally observed for 2 is shown in Fig. 2. Variation of the axial halide ligands induces a systematic shift in the resonant absorption of the ammine protons. The upfield shift in the resonances from 1 (5.87 pm) to 2 (5.84 ppm) to 3 (5.77 ppm) is consistent with greater shielding conveyed by the less electronegative halides.

As stated above, oxidation to Pt(IV) symmetrizes the electric field gradient of the ^{14}N nucleus, which permits direct observation of sharp ^{14}N NMR signals for **1** and **2**.[39] Fully coupled spectra could be obtained (Fig. S3), but proton-decoupling (Fig. S4 and S9) enhanced the signal-to-noise ratio and allowed platinum satellites to be clearly observed for both **1** and **2**. As observed for the ^{1}H NMR signals, the ^{14}N resonances shift upfield with change of the axial halide ligand from chloride to bromide, from −33.7 ppm to −40.9 ppm. The $^{1}J(^{14}\mathrm{N}–^{195}\mathrm{Pt})$ coupling constants do not vary significantly between **1** and **2**, which exhibit values of 177 Hz and 175 Hz, respectively. The magnitude of this coupling is related to hybridization at the platinum center and the nature of the ligand trans to the ammine.[51] The variation of less than 1.5% in the $^{1}J(^{14}\mathrm{N}–^{195}\mathrm{Pt})$ values of **1** and **2** is consistent with the lack of Pt rehybridization and the congruence of the ligand trans to the ammine.

^{195}Pt NMR spectroscopy provides a highly sensitive measure of coordination environment and oxidation state, and platinum complexes exhibit a chemical shift range of approximately 13000 ppm.[52] The significant downfield shift observed following treatment of cisplatin ($\delta \approx -2100$)[50] with iodobenzene dichloride, bromine, or iodine is consistent with oxidation of the Pt(II) center to the 4+ state.[53] As with the ^{1}H and ^{14}N spectroscopic experiments described above, the ^{195}Pt resonances shift with the halide ligands as follows: −123 ppm for **1**, −732 ppm for **2**, and −1866 ppm for **3**. In the theory developed by Ramsey and elaborated by others,[54] chemical shift is divided into a diamagnetic part and a paramagnetic part. Paramagnetic shielding is the dominant interaction in dictating changes to the chemical shift of the ^{195}Pt nucleus as a function of changing ligand field.[55] The degree of paramagnetic shielding afforded to a transition metal by its ligands follows the same trend as the position of those ligands in the nephelauxetic series;[56] the ^{195}Pt chemical shifts of **1**–**3** vary accordingly. More recent revisions of this theory have recognized the important contribution of spin-orbit coupling to the ^{195}Pt chemical shift.[57] The nephelauxetic series trend described above is a manifestation of this spin-orbit coupling effect, which increases as Cl < Br < I.[57]

The splitting pattern of the ^{195}Pt NMR signal expected from coupling to the two equivalent ^{14}N nuclei and the six equivalent protons is a pentet of septets. In general, efforts were not taken to resolve these couplings, but careful measurement and processing of the ^{195}Pt NMR spectrum of **2** permitted their full resolution at 86 MHz (Fig. 2). The coupling constants obtained from this spectrum are equivalent to those obtained independently from ^{1}H NMR spectra and consistent with those obtained from the ^{14}N NMR spectra of **1** and **2**. Similar trends were observed in the NMR spectra of the carboplatin prodrugs **4**–**6**.

X-ray crystallographic study of 1 and 3

cis,*cis*,*trans*-[$Pt(NH_3)_2Cl_2X_2$], where X = Cl or I, both crystallize from DMF with the same structural motif in which each platinum complex crystallizes with three DMF molecules. The ability this solvent to yield large crystals of *cis*-[$Pt(NH_3)_2Cl_2$]·DMF has been exploited as a means of purifying cisplatin.[58,59] The carbonyl fragments of the DMF molecules act as hydrogen bond acceptors for the platinum-bound ammine ligands. Hydrogen bonding metrics, determined using *PLATON*, are reported in the ESI (Tables S9–S18). In the structures of 1 and 3, the oxygen atom of one DMF forms hydrogen bonds with the two cis ammines of one platinum complex. The remaining two solvent molecules bridge symmetry-related platinum complexes. In the structure of 1·3DMF, these bridging DMF molecules form hydrogen-bonded chains that propagate along the *b* axis (Fig. 3). In the structure of 3·3DMF, there are two symmetry-independent platinum complexes within the asymmetric unit. Each has three DMF molecules associated with it and forms a hydrogen-bonding network similar to that described above. In both cases, the hydrogen bonded chains propagate along *b*. One set of chains has close I···I contacts (3.6472(6) Å), whereas the other does not and its closest I···I distance is 4.4321(7) Å (Fig. 3). Crystal structures containing more than one crystallographically independent molecule in the asymmetric unit can arise from frustration between different types of intermolecular interactions.[60] In this structure, such competition may be occurring between hydrogen bonding and the iodide–iodide interaction.

The cisplatin prodrugs **1** and **3** both have a pseudo-octahedral coordination geometry in which the core structure of the *cis*-diamminedichloroplatinum unit is maintained. The equatorial Pt–N and Pt–Cl bond lengths do not vary significantly from those in the structure of cisplatin.[61] The axial ligands form an X–Pt–X angle of 174.24(2)° for X = Cl (**1**) and 176.91(1)° and 179.06(1)° for the two crystallographically independent molecules of **3**, for which X = I. In each case, the axial ligands bend away from the equatorial chlorides toward the ammine ligands. The greater steric bulk of the equatorial chloride ligands compared to the ammines pushes the axial halides in this direction. As the length of the Pt–X bond of the axial ligands increases, this steric strain decreases and the X–Pt–X angle approaches 180°.

During the selection of a suitable sample of **1** for X-ray diffraction analysis, one single crystal of all those investigated microscopically had a slightly different color. Instead of the bright yellow characteristic of **1**·3DMF, it had a tint of orange, which was particularly evident when viewed under crossed polarizers. Diffraction analysis revealed this crystal to contain *fac*-[$Pt(NH_3)_3Cl_3$]Cl·DMF, which appears to have formed by decomposition during the extended crystallization time. A detailed analysis of the structure of this compound is not provided here but refinement details, a thermal ellipsoid plot, and the CIF are provided as ESI. We briefly note that it is only the fourth platinum compound to be deposited in the CSD containing a facial arrangement of three chloride and three N-donor ligands.[62-64] The crystal structure of *fac*-[$Pt(NH_3)_3Br_3$]Br·DMF was also obtained but is not discussed further (details in ESI). No other platinum compound with a facial coordination of three bromide and three N-donor ligands has been deposited in the CSD.

X-ray crystallographic study of 4 and 5

Crystal structures of the carboplatin prodrugs 4 and 5 were also solved. The crystals were obtained from DMF and, as with the cisplatin prodrugs described above, the two share common structural motifs. The carboplatin prodrugs, unlike the *cis*-diamminetetrahaloplatinum(IV) species, have carbonyl fragments from the CBDCA ligand that can serve as hydrogen bond acceptors for ammine ligands. The main structural motif is an inversion-related pair of complexes that form reciprocal hydrogen bonds (Fig. 4). These dimers generate chains through hydrogen bonding interactions with DMF. In the structures of both 4·DMF and 5·DMF, one of the ammine N–H bonds lacks a formal hydrogen bond acceptor, but is directed toward the axial halide of an adjacent complex. In the crystals containing 4, the N···Cl distance is 3.604(2) Å and the N–H–Cl angle is 173.7°. In the crystals containing 5, the N···Br distance is 3.817(2) Å and the N–H–Br angle is 168.4°.

The crystal structures also reveal some interesting molecular features. The malonate portion of the CBDCA ligand adopts a boat conformation in carboplatin.[65] The presence of a single set of CBDCA ^{1}H NMR spectral resonances is attributed to rapid flipping of the ligand from one boat conformer to the other in solution.[66] The conformational dynamics of carboplatin have been probed by investigating variable temperature solid state NMR spectra of carboplatin derivatives.[67] The boat conformation positions the CBDCA ring over one face of the platinum complex (Fig. 5), a feature that has been proposed to help protect the compound from deactivation by intracellular thiols.[68] In compounds **4**–**6**, the steric bulk of the axial halide ligands of the Pt(IV) prodrug push the cyclobutane ring away from the face of the platinum complex, forcing the malonate chelate ring into a flattened-boat conformation (Fig. 5). In the structures described here, five of the atoms are essentially coplanar. The flattening of the chelate ring can be quantitated by measuring the dihedral angle between the plane that best fits the platinum and ligated oxygen atoms and that which best fits the carbonyl and quaternary carbon atoms. These are the blue and red planes, respectively, in Fig. 5. The green plane in Fig. 5 is the plane that best fits the platinum-bound oxygen atoms and the carbonyl carbon atoms. The dihedral angle between the blue and red planes is 86° for carboplatin, 41° for **4**, and 36° for **5**. Although apparently not published, a crystal structure of **6** has been deposited in the CSD as a personal communication by Sadler and coworkers (CCDC 276866); the corresponding dihedral angle in this structure is 30°.

The flattening of the chelate ring appears to stem directly from a steric interaction between the halide and the cyclobutane ring and not from any change in the electronic structure of the compound induced upon oxidation to the 4+ state. This feature can be appreciated by examining the crystal structure of the carboplatin prodrug bearing axial hydroxide ligands, *cis*,*trans*-[Pt(CBDCA)$(NH_3)_2(OH)_2$] (details presented in the ESI). In this structure, the malonate ring again adopts a flattened-boat conformation but the platinum atom, as opposed to the quaternary carbon, is displaced from the plane formed by the other five atoms. This difference from the complexes with axial halides most likely arises because of the shorter metal-ligand bond and smaller effective radius of the hydroxide ligand. Further corroboration of the proposal that these changes in the CBDCA conformation observed in these crystal structures arise from intramolecular, as opposed to intermolecular, interactions

was provided by computational studies using DFT methods. Geometry optimization in the gas phase reproduced the general structural features of carboplatin and complexes **4**–**6** that were determined by X-ray crystallography. These features include the boat conformation of the malonate portion of the CBDCA ligand of carboplatin and the flattened-boat conformations of the CBDCA ligands of the Pt(IV) prodrugs. The RMSD of the non-H atoms of the calculated and experimental structures for **4**, **5**, and **6** are 0.12 Å, 0.13 Å, and 0.26 Å, respectively. These computed structures of **4**–**6** support the hypothesis that, as the radius of the halide ligand increases, the malonate ring of the CBDCA ligand is pushed toward a planar conformation.

Crystal structure of 7·3DMF·Et_2O

There are examples of amido-bridged complexes of platinum(II),[69-72] platinum(III),[39,73] and platinum(IV)[48,49] that have been characterized spectroscopically and crystallographically. In these systems, crystallographic characterization often requires careful consideration. For instance, reanalysis of the structure of a head-to-tail tetranuclear Pt(III) complex initially formulated[74] as $[(H_2O)(H_3N)_2Pt(\mu\text{-}C_4H_6NO)_2Pt(NH_3)(\mu\text{-}OH_2)]_2$ revealed that the bridging hydroxide ligands are most likely bridging amide ligands.[39] Analysis of the hydrogen bonding patterns in the crystal structure of 7·3DMF·Et_2O confirms that the bridging ligands are amides in both crystallographically independent dimers. The calculated Z value of 2 suggested one dimer in the asymmetric unit centered on a general position. Solution of the structure revealed instead the presence of two crystallographically independent half-dimers on different inversion centers. A parameter typically used to describe the number of independent molecules within the asymmetric unit is Z′,[75] defined as the number of formula units in the unit cell divided by the multiplicity of a general position in the space group. This definition, however, does not account for cases in which molecules sit on crystallographically distinct special positions. In the case of the structure of 7·3DMF·Et_2O, Z′ = 1, but the crystal clearly contains two crystallographically independent molecules. In the extended Z′ descriptor notation, developed to handle cases of this sort, this structure would be described as having Z′ = ½ + ½. In the notation developed by Zorkii and Bel'skii, the structure class symbol for this crystal structure is *P*, Z = 2(,), where the numbers in parentheses represent the site-symmetries of the distinct special position upon which the crystallographically independent molecules sit.[76] An analysis of the structures deposited in the CSD revealed the relative occurrence of crystal structures in which molecules sit upon distinct special positions.[77] Although this phenomenon is rare, the case in which the molecule crystallizes in space group *P* with two molecules sitting on different inversion centers is its most common manifestation.[77]

Care must be taken to ensure that a shift of the origin or reduction of unit cell size will not reveal these two half molecules to be crystallographically related. In the present structure, the two molecules engage in distinct hydrogen bonding patterns. In one dimer, the two hydrogen atoms of the bridging amide are directed toward the carbonyl moieties of DMF molecules. In the other, one amide hydrogen atom is directed toward a DMF carbonyl and the other is directed toward the carbonyl of the CBDCA ligand from a neighboring complex. Moreover, the cyclobutane ring of one of the half-dimers in the asymmetric unit is disordered across the two pucker conformations, whereas the other is well ordered. With the

exception of a differential puckering of the cyclobutane ring, the structures of the two crystallographically independent dimers are essentially identical. Because one of the Pt–N bonds of the bridging amide is trans to a strongly *trans*-directing iodide ligand and the other is trans to a carboxylate, the Pt_2N_2 rhomb is not equilateral. For the two crystallographically independent molecules, the length of the Pt–N bond trans to the iodide is 2.066(5)/2.058(3) Å and that of the bond trans to carboxylate is 2.028(3)/2.020(3) Å. As expected, the platinum atoms are sufficiently far apart, 3.1100(3)/3.0910(4) Å, that there is no covalent interaction between them.

Conclusions

The Pt(IV) prodrug approach holds significant promise for the development of novel platinum-based anticancer agents of clinical value. The work described here provides a synthetic framework for the facile preparation of prodrugs bearing axial chloride ligands or axial halides different from those commonly encountered in the literature. This synthetic methodology can be used to obtain complexes intended for direct application to biological systems or as synthetic intermediates in the preparation of more complex platinum-containing molecules. A detailed analysis of the variation in the spectroscopic and structural properties induced by altering the axial halide was presented. The ability to systematically alter these properties allows chemists to endow a platinum complex with precise attributes necessary for a given biological function. The methodologies presented here expand the toolkit of synthetic bioinorganic chemists, facilitating such designed syntheses.

Supplementary Material

Refer to Web version on PubMed Central for supplementary material.

Acknowledgments

This work was supported by the NCI under grant CA034992.

References

1. Wheate NJ, Walker S, Craig GE, Oun R. Dalton Trans. 2010; 39:8113–8127. [PubMed: 20593091]
2. Rosenberg B, VanCamp L, Trosko JE, Mansour VH. Nature. 1969; 222:385–386. [PubMed: 5782119]
3. Wong E, M C. Giandomenico, Chem. Rev. 1999; 99:2451–2466.
4. Sternberg CN, Petrylak DP, Sartor O, Witjes JA, Demkow T, Ferrero J-M, Eymard J-C, Falcon S, Calabrò F, James N, Bodrogi I, Harper P, Wirth M, Berry W, Petrone ME, McKearn TJ, Noursalehi M, George M, Rozencweig M. J. Clin. Oncol. 2009; 27:5431–5438. [PubMed: 19805692]
5. Johnstone TC, Wilson JJ, Lippard SJ. Inorg. Chem. 2013; 52:12234–12249. [PubMed: 23738524]
6. Hall MD, Mellor HR, Callaghan R, Hambley TW. J. Med. Chem. 2007; 50:3403–3411. [PubMed: 17602547]
7. Wexselblatt E, Gibson D. J. Inorg. Biochem. 2012; 117:220–229. [PubMed: 22877926]
8. Nemirovski A, Vinograd I, Takrouri K, Mijovilovich A, Rompel A, Gibson D. Chem. Commun. 2010; 46:1842–1844.
9. Lemma K, Berglund J, Farrell N, Elding LI. J. Biol. Inorg. Chem. 2000; 5:300–306. [PubMed: 10907740]
10. Lemma K, Shi TS, Elding LI. Inorg. Chem. 2000; 39:1728–1734. [PubMed: 12526561]

11. Wilson JJ, Lippard SJ. Chem. Rev. 2013; 114:4470–4495. [PubMed: 24283498]
12. Giandomenico CM, Abrams MJ, Murrer BA, Vollano JF, Rheinheimer MI, Wyer SB, Bossard GE, Higgins JD III. Inorg. Chem. 1995; 34:1015–1021. [PubMed: 20000850]
13. Wilson JJ, Lippard SJ. Inorg. Chem. 2011; 50:3103–3115. [PubMed: 21361279]
14. Ellis LT, Er HM, Hambley TW. Aust. J. Chem. 1995; 48:793–806.
15. Kauffman GB, Slusarczuk G, Kirschner S. Inorg. Synth. 1963; 7:236–238.
16. Rochon FD, Gruia LM. Inorg. Chim. Acta. 2000; 306:193–204.
17. Varbanov HP, Valiahdi SM, Kowol CR, Jakupec MA, Galanski M, Keppler BK. Dalton Trans. 2012; 41:14404–14415. [PubMed: 22886297]
18. An upgrade in the NMR instrumentation of the MIT DCIF removed the probe that was capable of observing ^{14}N
19. Zhao XF, Zhang C. Synthesis. 2007:551–557.
20. Bruker. APEX2. Bruker AXS Inc.; Madison, Wisconsin: 2008.
21. Bruker. SAINT: SAX Area-Detector Integration Program. Bruker AXS Inc.; Madison, Wisconsin: 2008.
22. Bruker. SADABS: Area-Detector Absorption Correction. Bruker AXS Inc.; Madison, Wisconsin: 2001.
23. Bruker. XPREP. Bruker AXS Inc.; Madison, Wisconsin: 2008.
24. Sheldrick GM. Acta Crystallogr. Sect. A. 2008; 64:112–122. [PubMed: 18156677]
25. Müller P. Crystallogr. Rev. 2009; 15:57–83.
26. Spek AL. J. Appl. Crystallogr. 2003; 36:7–13.
27. Macrae CF, Edgington PR, McCabe P, Pidcock E, Shields GP, Taylor R, Towler M, van de Streek J. J. Appl. Crystallogr. 2006; 39:453–457.
28. Frisch, MJ.; Trucks, GW.; Schlegel, HB.; Scuseria, GE.; Robb, MA.; Cheeseman, JR.; Montgomery, J.; Vreven, T.; Kudin, KN.; Burant, JC.; Millam, JM.; Iyengar, SS.; Tomasi, J.; Barone, V.; Mennucci, B.; Cossi, M.; Scalmani, G.; Rega, N.; Petersson, GA.; Nakatsuji, H.; Hada, M.; Ehara, M.; Toyota, K.; Fukuda, R.; Hasegawa, J.; Ishida, M.; Nakajima, T.; Honda, Y.; Kitao, O.; Nakai, H.; Klene, M.; Li, X.; Knox, JE.; Hratchian, HP.; Cross, JB.; Adamo, C.; Jaramillo, J.; Gomperts, R.; Stratmann, RE.; Yazyev, O.; Austin, AJ.; Cammi, R.; Pomelli, C.; Ochterski, JW.; Ayala, PY.; Morokuma, K.; Voth, GA.; Salvador, P.; Dannenberg, JJ.; Zakrzewski, VG.; Dapprich, S.; Daniels, AD.; Strain, MC.; Farkas, O.; Malick, DK.; Rabuck, AD.; Raghavachari, K.; Foresman, JB.; Ortiz, JV.; Cui, Q.; Baboul, AG.; Clifford, S.; Cioslowski, J.; Stefanov, BB.; Liu, G.; Liashenko, A.; Piskorz, P.; Komaromi, I.; Martin, RL.; Fox, DJ.; Keith, T.; Al-Laham, MA.; Peng, CY.; Nanayakkara, A.; Challacombe, M.; Gill, PMW.; Johnson, B.; Chen, W.; Wong, MW.; Gonzalez, C.; Pople, JA. Gaussian 03. Gaussian, Inc.; Pittsburgh PA: 2003. J. A.
29. Adamo C, Barone V. J. Chem. Phys. 1999; 110:6158–6170.
30. Hay PJ, Wadt WR. J. Chem. Phys. 1985; 82:270–283.
31. Hay PJ, Wadt WR. J. Chem. Phys. 1985; 82:299–310.
32. Ditchfield R, Hehre WJ, Pople JA. J. Chem. Phys. 1971; 54:724–728.
33. Hehre WJ, Ditchfield R, Pople JA. J. Chem. Phys. 1972; 56:2257–2261.
34. Brandon RJ, Dabrowiak JC. J. Med. Chem. 1984; 27:861–865. [PubMed: 6330359]
35. Kratochwil NA, Bednarski PJ, Mrozek H, Vogler A, Nagle JK. Anti-Cancer Drug Des. 1996; 11:155–171.
36. Ravera M, Gabano E, Pelosi G, Fregonese F, Tinello S, Osella D. Inorg. Chem. 2014 DOI: 10.1021/ic501446b.
37. Guo S-X, Mason DN, Turland SA, Lawrenz ET, Kelly LC, Fallon GD, Gatehouse BM, Bond AM, Deacon GB, Battle AR, Hambley TW, Rainone S, Webster LK, Cullinane C. J. Inorg. Biochem. 2012; 115:226–239. [PubMed: 22921430]
38. Wilson JJ, Lippard SJ. Inorg. Chim. Acta. 2012; 389:77–84.
39. Wilson JJ, Lippard SJ. Inorg. Chem. 2012; 51:9852–9864. [PubMed: 22946515]
40. Wilson JJ, Lippard SJ. Polyhedron. 2013; 58:71–78. [PubMed: 24489429]

41. Lucas HJ, Kennedy ER, Johnson JR, Formo MW. Org. Synth. 1942; 22:69.
42. Zanka A, Takeuchi H, Kubota A. Org. Process Res. Dev. 1998; 2:270–273.
43. Knight DW, Russell GA. 2001 e-EROS Encycl. Reagents Org. Synth.
44. Jones MM, Morgan KA. J. Inorg. Nucl. Chem. 1972; 34:259–274.
45. Tamasi G, Cini R, Intini FP, Sivo MF, Natile G. Angew. Chem., Int. Ed. 2004; 43:5081–5084.
46. Margiotta N, Ranaldo R, Intini FP, Natile G. Dalton Trans. 2011; 40:12877–12885. [PubMed: 22064914]
47. Kratochwil NA, Zabel M, Range K-J, Bednarski PJ. J. Med. Chem. 1996; 39:2499–2507. [PubMed: 8691447]
48. Kretschmer M, Heck L, Anorg Z. Allg. Chem. 1982; 490:215–229.
49. Frank W, Heck L, Müller-Becker S, Raber T. Inorg. Chim. Acta. 1997; 265:17–22.
50. Still BM, Kumar PGA, Aldrich-Wright JR, Price WS. Chem. Soc. Rev. 2007; 36:665–686. [PubMed: 17387413]
51. Appleton TG, Hall JR, Ralph SF. Inorg. Chem. 1985; 24:4685–4693.
52. Pregosin PS. Coord. Chem. Rev. 1982; 44:247–291.
53. Kidd RG. Annu. Rep. NMR Spectrosc. 1991; 23:85–139.
54. Pyykkö P. Theor. Chem. Acc. 2000; 103:214–216.
55. Juranić N. Coord. Chem. Rev. 1989; 96:253–290.
56. Juranić N. J. Am. Chem. Soc. 1988; 110:8341–8343.
57. Gilbert TM, Ziegler T. J. Phys. Chem. A. 1999; 103:7535–7543.
58. Raudaschl G, Lippert B, Hoeschele JD. Inorg. Chim. Acta. 1983; 78:L43–L44.
59. Raudaschl G, Lippert B, Hoeschele JD, Howard-Lock HE, Lock CJL, Pilon P. Inorg. Chim. Acta. 1985; 106:141–149.
60. Anderson KM, Afarinkia K, Yu H.-w. Goeta AE, Steed JW. Cryst. Growth Des. 2006; 6:2109–2113.
61. Ting VP, Schmidtmann M, Wilson CC, Weller MT. Angew. Chem. 2010; 49:9408–9411. [PubMed: 21031378]
62. Britten JF, Lock CJL. Acta Crystallogr. Sect. B. 1980; 36:2958–2963.
63. Khripun AV, Haukka M, Nikolaeva DN, Kukushkin V. Yu. Acta Crystallogr. Sect. E. 2005; 61:m2069–m2071.
64. Xue Z, Kuzuhara D, Ikeda S, Okujima T, Mori S, Uno H, Yamada H. Inorg. Chem. 2013; 52:1688–1690. [PubMed: 23379254]
65. Beagley B, Cruickshank DWJ, McAuliffe CA, Pritchard RG, Zaki AM, Beddoes RL, Cernik RJ, Mills OS. J. Mol. Struct. 1985; 130:97–102.
66. Neidle S, Ismail IM, Sadler PJ. J. Inorg. Biochem. 1980; 13:205–212.
67. Guo Z, Habtemariam A, Sadler PJ, Palmer R, Potter BS. New J. Chem. 1998; 22:11–14.
68. Dabrowiak, JC. Metals in Medicine. Wiley, Hoboken; 2009. p. 109-147.
69. Alcock NW, Bergamini P, Kemp TJ, Pringle PG, Sostero S, Traverso O. Inorg. Chem. 1991; 30:1594–1598.
70. Park S, Rheingold AL, Roundhill DM. Organometallics. 1991; 10:615–623.
71. Schneider A, Freisinger E, Beck B, Lippert B. J. Chem. Soc., Dalton Trans. 2000:837–838.
72. Beck B, Schneider A, Freisinger E, Holthenrich D, Erxleben A, Albinati A, Zangrando E, Randaccio L, Lippert B. Dalton Trans. 2003:2533–2539.
73. Matsumoto K, Harashima K. Inorg. Chem. 1991; 30:3032–3034.
74. Sakai K, Tanaka Y, Tsuchiya Y, Hirata K, Tsubomura T, Iijima S, Bhattacharjee A. J. Am. Chem. Soc. 1998; 120:8366–8379.
75. Anderson KM, Steed JW. CrystEngComm. 2007; 9:328–330.
76. Zorkii PM, Bel'skii VK, Lazareva SG, Porai-Koshits MA. J. Struct. Chem. 1967; 8:267–270.
77. Bond AD. CrystEngComm. 2008; 10:411–415.

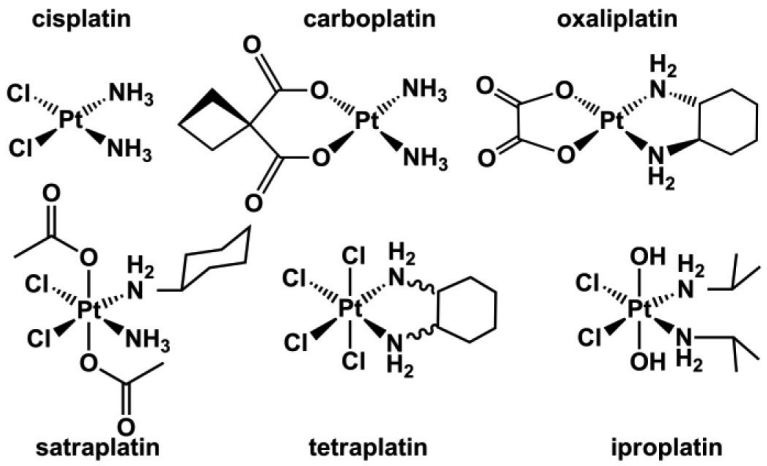

Chart 1.
Selection of Pt(II) (top) and Pt(IV) complexes (bottom) investigated in a clinical setting.

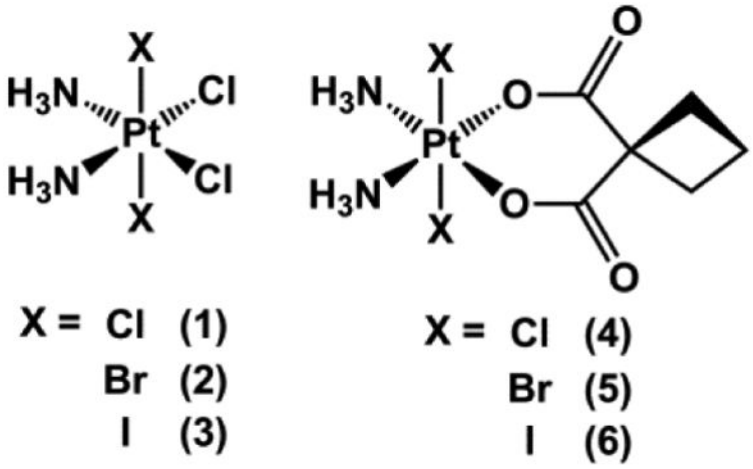

Chart 2.
The target Pt(IV) prodrugs of cisplatin, **1**–**3**, and carboplatin, **4**–**6**.

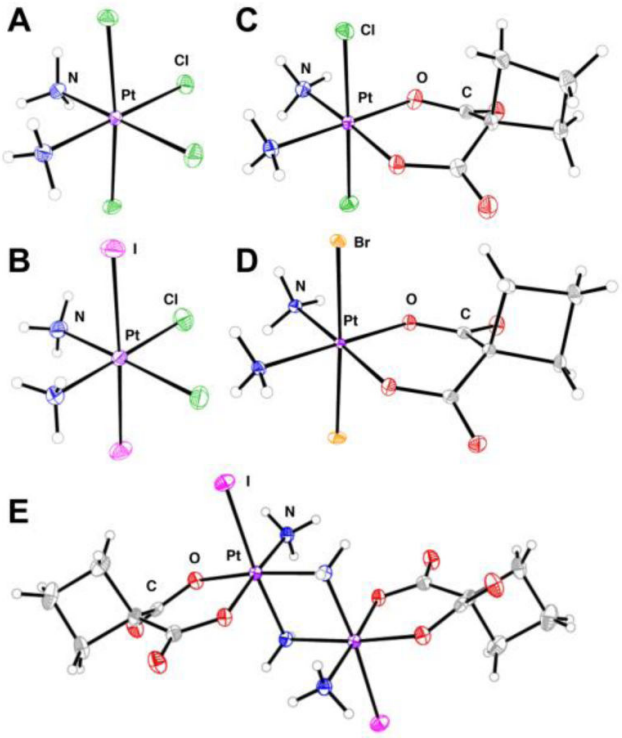

Fig. 1.

Molecular structures of platinum complexes from the crystal structures of a) **1**, b) **3**, c) **4**, d) **5**, and e) **7**. Thermal ellipsoids are shown at the 50% probability level and hydrogen atoms are shown as spheres of arbitrary radius. Color code: Purple Pt, blue N, red O, grey C, magenta I, orange Br. For b) and e) only one of the two crystallographically independent molecules present in the asymmetric unit is shown.

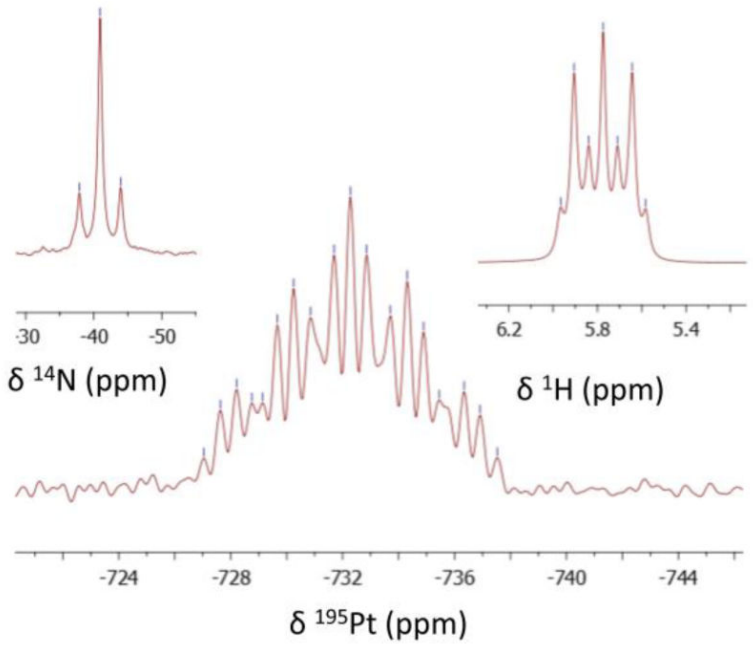

Fig. 2.

NMR spectra (11.7 T) of **2** showing the coupling between the ^{1}H, ^{14}N, and ^{195}Pt nuclei. The ^{14}N spectrum is proton-decoupled to allow the platinum satellites to show more readily. Fully annotated spectra are presented in the ESI.

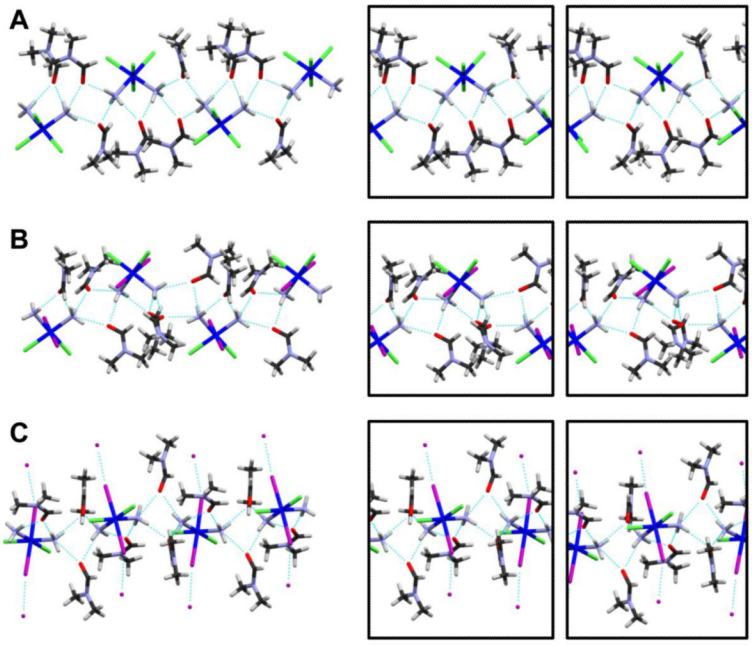

Fig. 3.

Crystallographic intermolecular interactions in (a) **1** and (b, c) the two crystallographically independent molecules of **3**. Hydrogen bonding between the platinum complexes and DMF solvent molecules is indicated by dotted blue lines. One of the molecules of **3** also participates in close I···I contacts as shown with blue dotted lines in (c). Boxed at the right are stereo images of the repeating unit of each motif. Color code: Dark blue Pt, green Cl, purple I, light blue N, red O, grey C, white H.

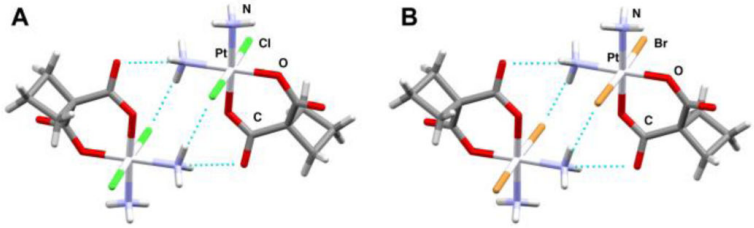

Fig. 4.

Intermolecular interactions in the crystal structures of **4** (a) and **5** (b) shown as blue dotted lines. Color code: Silver Pt, green Cl, orange Br, blue N, red O, grey C, white H.

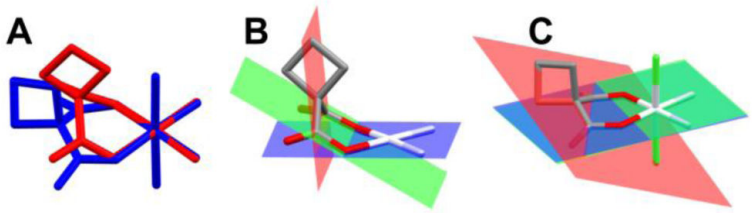

Fig. 5.

a) Overlay of the crystallographically determined structures of carboplatin (red) and **1** (blue). b) Planes of best fit indicating the boat conformation of the CBDCA ligand of carboplatin. c) Planes of best fit indicating the flattened-boat conformation of the CBDCA ligand of **1**. The atoms through which the planes are chosen to pass are described in the main text.

Table 1

Crystallographic parameters for 1·3DMF, 3·3DMF, 4·DMF, 5·DMF, and 7·3DMF-Et_20

	1·3DMF	3·3DMF	4-DMF	5-DMF	7-3DMF-Et20
Formula	$C_9H_{27}C1_4N_5O_3Pt$	$C_9H_{27}Cl_2I_2N_5O_3Pt$	$C_9H_{19}C1_2N_3O_5Pt$	$C_9H_{19}Br_2N_5O_5Pt$	$C_{22}H_{53}I_2N_7O_{12}Pt_2$
FW	590.25	773.15	515.26	604.18	1287.72
Space group	$P2_1/c$	$P2_1/c$	$P\bar{1}$	$P\bar{1}$	$P\bar{1}$
a, Å	10.0850(4)	21.974(3)	8.0456(5)	8.1817(4)	13.0123(11)
b, Å	12.9560(5)	12.4000(14)	10.2110(6)	9.5209(5)	13.2677(11)
c, Å	16.0513(6)	17.573(2)	10.2604(6)	11.4203(5)	13.388(2)
α, °			98.438(1)	108.009(1)	94.816(2)
β, °	104.918(1)	112.003(2)	104.454(1)	107.490(1)	100.174(2)
γ, °			106.933(1)	95.406(1)	118.650(1)
V, $Å^3$	2026.59(14)	4439.6(9)	758.64(8)	789.55(7)	1958.0(4)
Z	4	8	2	2	2
T, K	100(2)	100(2)	100(2)	100(2)	100(2)
μ(Mo Kα), mm^{-1}	7.466	9.358	9.621	13.967	8.775
θ range, °	2.05 to 28.33	1.92 to 28.97	2.11 to 28.28	2.00 to 28.70	1.58 to 28.37
total data	40197	88414	14758	15848	38217
unique data	5046	11675	3744	4040	9716
parameters	207	413	185	185	453
completeness (%)	99.9	99.3	99.2	99.3	99.2
R_1[a] (%)	1.30	2.63	1.27	1.88	2.27
wR_2[b] (%)	3.01	6.52	3.10	5.12	4.52
GoF[c]	1.086	1.077	1.064	1.134	1.031

[a] $R_1 = \Sigma||F_o| - |F_c|| / \Sigma|F_o|$.

[b] $wR_2 = \{\Sigma[w(F_o^2 - F_c^2)^2] / \Sigma[w(F_o^2)^2]\}^{1/2}$.

[c] $GoF = \{\Sigma[w(F_o^2 - F_c^2)^2] / (n-p)\}^{1/2}$